

Chapter 1

Experimental Background

In this chapter, experimental techniques that are used in my research will be described briefly as a practical guide for those who want to test or perform some parts of the experiments in this thesis. The following aspects will be covered:

- *Escherichia coli* (*E. coli*) bacterial suspensions are the model system throughout the whole thesis, so I will start talking about the preparation of motile bacterial sample in Sec. 1.1.
- Optical microscopy along with digital imaging has been the key approach for investigating how the microscopic dynamics lead to macroscopic property difference. The standard operations of imaging equipments have been documented by the equipment manufacturer already. In Sec. 1.2, I describe some practical challenges I have encountered when performing the experiments in this thesis and how I overcame them.
- The imaging approach we adopt naturally demands automated image analysis tools. In Sec. 1.3, I will describe the image analysis techniques I used.
- When investigating the rheology of bacterial suspensions, we adopted a homemade

microfluidic viscometer device. Details of the fabrication are shown in Sec. 1.4.

- A light-powered *E. coli* strain is used in the giant number fluctuations study and the emergence of active turbulence study (Chap. ?? and Chap. ??). This special strain was obtained by transforming a wild-type strain with an exogenous plasmid which encodes a light-harvesting membrane protein. The discovery and working principles of the light-powering feature has been well documented by earlier works [1, 2, 3, 4, 5]. Following these works, I constructed a plasmid containing the gene and successfully transformed the wild-type *E. coli* strain. In Sec. 1.5, I will present the details on the materials and procedures I used to construct the mutant as a practical guide to those who need to further modify or trouble shoot the strain I made.

1.1 Motile Bacteria Sample Preparation

Peritrichous *E. coli* bacteria have been widely used as model micro-swimmers for active fluid studies [6, 7]. By bundling and unbundling their flagella, they achieve a so called “run-and-tumble” motion, allowing them to more efficiently explore their surrounding environment and to search for supplies. Fig. 1.1a shows a simplified model of a swimming *E. coli* bacterium model with a 2 μm rod-shape body and a helical-shape flagellum of around 8 μm . When swimming, all the flagella bundle together behind the cell and propel it forward [8]. Fig. 1.1b and c show the bundled state and unbundled state of the flagella, respectively. A swimming *E. coli* bacterium can generate nontrivial fluid flow, which can lead to hydrodynamic attraction to boundaries, alignment with other bacteria and other consequences [9]. It had long been assumed in theoretical works that the effective flow generated by microswimmers like *E. coli* is dipolar, with one force pushing forward from the head and another force pushing backward from the flagella

[10, 11, 12, 13]. This assumption was then experimentally verified by Drescher et al. in 2011 [14], by reconstructing the flow field from many tracer particle trajectories. Fig. 1.1d and e show the flow field they measured and the best-fit force dipole flow. As I will show later, the swimming-induced flow plays a key role in the novel properties and collective motions in the bacterial active fluids.

There are quite a few research groups over the world that are using *E. coli* suspensions to study active fluids. To name a few, Yodh and Arratia at University of Pennsylvania, Wu at Cornell University, Poon at the University of Edinburgh and Clement at ESPCI all have published experimental works using *E. coli* [16, 17, 18, 19, 20]. Although the protocols of preparing motile *E. coli* samples are similar across different groups' protocols, they have subtle differences from each other, which may be attributed to the specific strain of *E. coli*, ingredients of media and specific instrument conditions. Schwarz-Linek et al. proposed a sample preparation protocol based on standard bio-science manuals [21] and Berg's *E. coli* protocol. If one wants to learn how to prepare motile *E. coli* from scratch, it is recommended to follow the protocol in Ref. [7].

When I joined the Cheng group at the University of Minnesota in 2015, before Ref. [7] was published, there was already a protocol in our lab that worked pretty well for us. I learned the protocol from previous lab members Yi Peng and Devranjan Samanta, and have made some modifications over the years to optimize the motility and concentration of samples and to include the additional procedures for preparing light-powered *E. coli*. Below I describe the protocol that works the best in Cheng lab.

1.1.1 Background Information

Bacterial strains We primarily work on two *E. coli* strains: *AW804* and *BW25113*.

AW804 is light-sensitive. *BW25113* is a wild type strain carrying a plasmid encoding green fluorescence protein, thus it is used when fluorescence / confocal

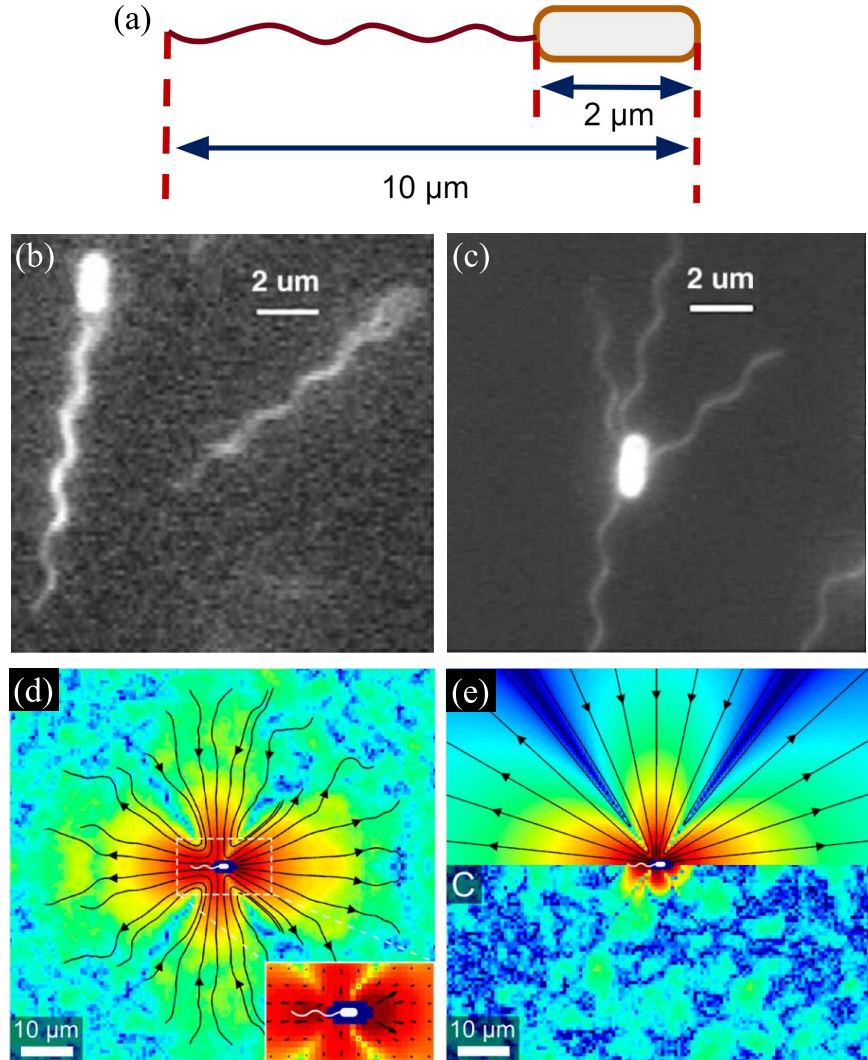


Figure 1.1: **Model swimmer *Escherichia coli* and its flow field.** (a) A schematic of a swimming *E. coli* bacterium. (b) Fluorescence microscopic image of swimming *E. coli* with bundled flagella. (c) Fluorescence microscopic image of tumbling *E. coli* with unbundled flagella. (d) Flow field around a swimming *E. coli*, measured with suspending microspheres. (e) Best-fit force dipole flow for the flow field shown in (d). Image sources: (b) and (c) are reproduced from Fig. 4a and 2a in Ref. [15] with permission from XXX. (d) and (e) are reproduced from Fig. 1a and 1b in Ref. [14] with permission from XXX.

microscopy is needed. Both strains have ampicillin resistance marker and thus require supplementing ampicillin to culturing media.

Antibiotics Bacteria are ubiquitous in the environment and can easily contaminate our bacterial culture. In order to ensure the fidelity of the culture, we add antibiotic resistance markers to the bacteria we want to grow and meanwhile add antibiotics to the medium. The antibiotics inhibit the growth of contaminating species and allow our desired bacteria to grow normally.

Medium Various types of media (terrific broth, Luria broth, 2XYT and M9, etc.) are commonly used for bacterial culture. We use terrific broth. The recipe can be found in the protocol section.

1.1.2 Protocol

1. Prepare a 2-ml *E. coli* overnight culture.

- (a) Prepare liquid terrific broth (TB). For example, to make 1 L TB, weigh out the following into a 1 L glass bottle:

- 23.6 g Yeast extract (Sigma-Aldrich)
- 11.8 g Tryptone plus (Sigma-Aldrich)
- 4 ml Glycerol (XXX)
- Add dI water to 1 L

Loosely close the cap on the bottle (do NOT close all the way or the bottle may explode!) and then loosely cover the top of the bottle with autoclave tape (stick cap and bottle body together to avoid cap popping off). Autoclave and allow to cool to room temperature. Now screw on the top of the bottle and store the TB at room temperature.

- (b) Using a sterile 10 ml pipette, transfer 2 ml TB to a sterile glass test tube.
 - (c) Using a sterile pipette, add 2 microliter (0.1% v/v) antibiotic solution to the TB in test tube.
 - (d) Using a sterile pipette tip, pick a small chunk from our bacterial frozen stock (stored in the -80 °C freezer in 251) and carefully transfer the small chunk into the liquid TB + antibiotic.
 - (e) Loosely cover the culture with sterile cap that is not air tight.
 - (f) Incubate bacterial culture at 37 °C for 12-18 h in a shaking incubator.
 - (g) After incubation, check growth, which is characterized by a cloudy haze in the media. This is the overnight culture.
2. Dilute overnight culture and harvest motile bacteria at mid-late log phase.
 - (a) Using a sterile 10 ml pipette, transfer 3 ml TB to a sterile glass test tube.
 - (b) Using a sterile pipette, add 2 microliter (0.1% v/v) antibiotic solution to the TB in test tube.
 - (c) Transfer 30 microliter (1% v/v) overnight culture into the liquid TB + antibiotic.
 - (d) Incubate bacterial culture at 30 °C for 6-6.5 h in a shaking incubator.
 - (e) After incubation, check for growth, which is characterized by a cloudy haze in the media. This is the log phase bacteria.
 3. Centrifuge for better motility and higher concentration bacterial sample.

- (a) Prepare motility buffer (MB), the following recipe is from Ref. [22].
 - 0.01 M potassium phosphate (combine monobasic and dibasic solutions, Sigma-Aldrich)

- 10^{-4} M EDTA (Sigma-Aldrich)
 - 0.002% weight fraction Tween 20 (Sigma-Aldrich)
 - Adjust pH to 7.0
- (b) Take out the log phase bacteria from the shaking incubator, centrifuge for 5 min at 800 rcf.
- (c) Discard the supernatant quickly and transfer the left-over liquid to a new centrifuge tube.
- (d) Add 500-1000 ul MB (or water) to resuspend the bottom pellet (avoid bottom pellet) and centrifuge for a second time (5 min, 800 rcf).
- (e) Discard the supernatant and let the tubes sit for two minutes. The remaining left-over liquid should be now filled with the active *E. coli*. Take the left-over solution in another capsule and use it for experiments.
- (f) To measure the concentration, transfer 10 microliter of the suspension into a 1 ml plastic cuvette (0.5 cm) and dilute 100 times (by adding 990 microliter water). Put the cuvette in the spectrophotometer (Eppendorf) and use the OD600 program. The resulting number times 100 will be the number density of your suspension in the unit of n_0 (8×10^8 cells/ml).

1.2 Optical Microscopy

In this section, I will describe how I overcome practical challenges when applying optical microscopy on bacterial suspensions. I want to note that the standard manuals are always the best reference for beginners who have just started to learn about a technique. In my case, the standard manuals are the Nikon inverted microscope Eclipse Ti-E Ti-E/B instructions [23], OpenPIV official website [24, 25] and trackpy official website [26].

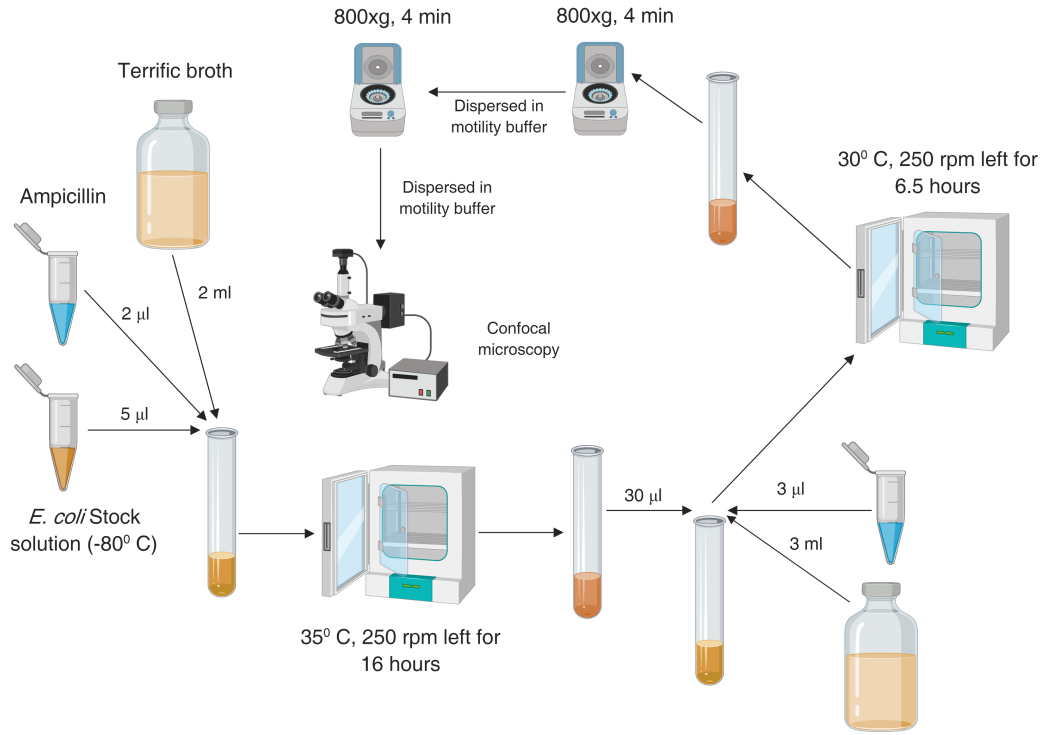


Figure 1.2: **Graphical motile *E. coli* sample preparation protocol.** Image courtesy of Shashank Kamdar.

Some related projects (listed in the websites mentioned) also provide valuable tutorials and ideas, for example the particle tracking routines in IDL by Crocker and Weeks [27] and in Matlab by Blair and Dufresne [28].

1.2.1 Power *E. coli* with Illumination Light

In the studies of the giant number fluctuations and the emergence of active turbulence, I used a light-powered *E. coli* mutant, which changes its swimming speed according to the amount of light it receives (details of the light-powered *E. coli* mutant can be found in Sec. 1.5).

I use the illumination light of the microscope as the power source of the bacteria,

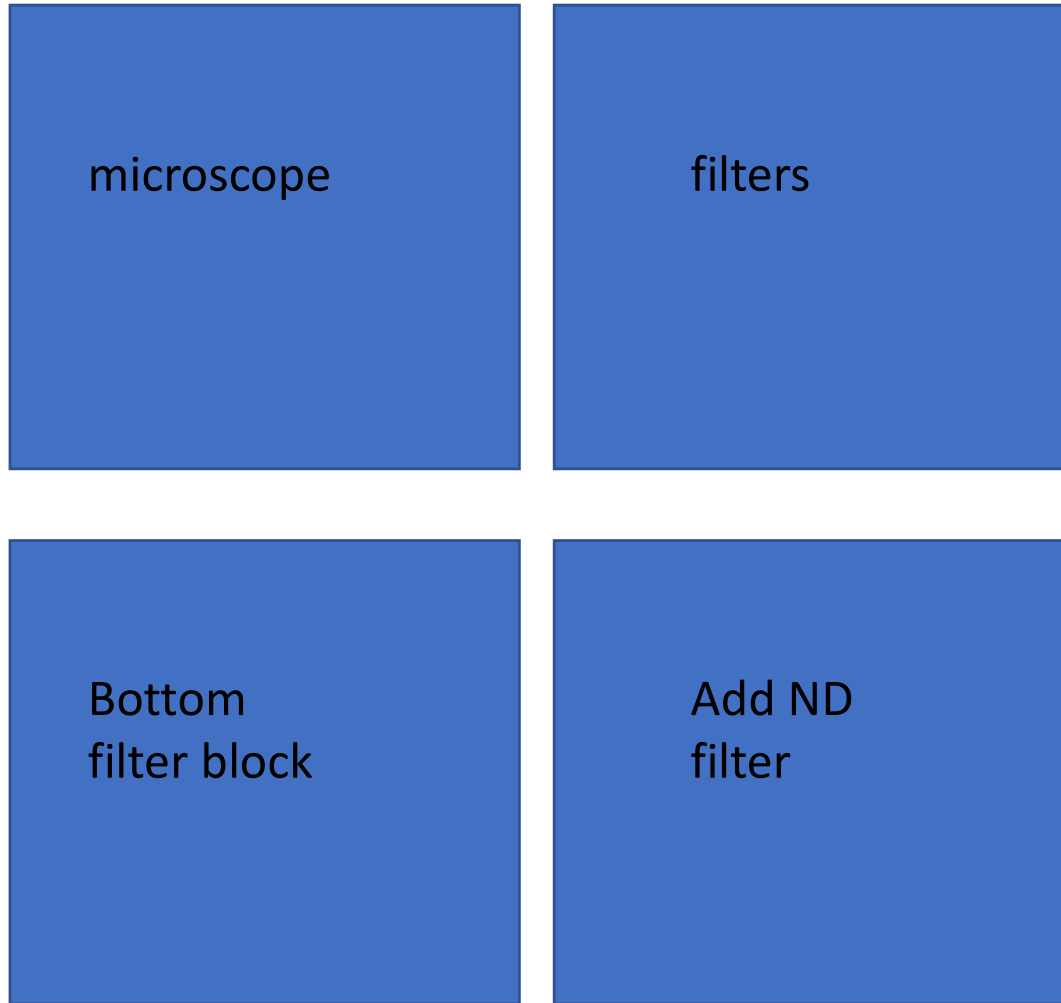


Figure 1.3: **Nikon Ti-E inverted microscope and its filters.** (a) Nikon Ti-E inverted microscope model. (b) Illumination light path filters. (c) Filter block under objective. (d) Adding additional ND filter under objective.

instead of using another light source, based on two considerations: 1) an additional light source shining on the sample will lead to additional unexpected light going into the objective, which often leads to bad image quality, 2) it is hard to construct a spatially uniform light, especially when it has to come in an angle not perpendicular to the specimen. Therefore, I use the illumination light of the microscope to power the *E. coli*.

The light-powered *E. coli* mutant requires quite a high light intensity to move fast enough. Such a high intensity cannot be achieved in the normal microscopy conditions, where four light filters are applied for different purposes. Fig. 1.3a and b show the Nikon Ti-E inverted microscope and the illumination light filtering system with the four light filters designated as ND, D, NCB and PFS. The functions of the filters are listed in Table. 1.1:

| | |
|------------|--|
| ND | Neutral density filter: adjust the brightness for normal microscopy or photomicroscopy |
| D | Diffusion filter: made of frosted glass and will diffuse light, used for equalizing the illumination |
| NCB | Neutral color balance: corrects the color temperature for normal microscopy or filming by daylight type color. Note: this filter is essential for optimal color reproducibility when taking color images, and it should be kept out of the optical path when filming in black and white. |
| PFS | Perfect focusing system: a hardware solution to combat axial focus fluctuations in real time during long-term imaging investigations. Note - this filter should be kept out if one does not intend to use the perfect focusing system. |

Table 1.1: Filters in the illumination light path and their functions.

Removing some of those filters can make the illumination light strong enough to power the bacteria. According to the functions of the filters, the only necessary filter is the diffusion filter, given that one is not doing color imaging and is not using perfect focusing system, as it is in my experiment. Fig. 1.4a shows an image taken without

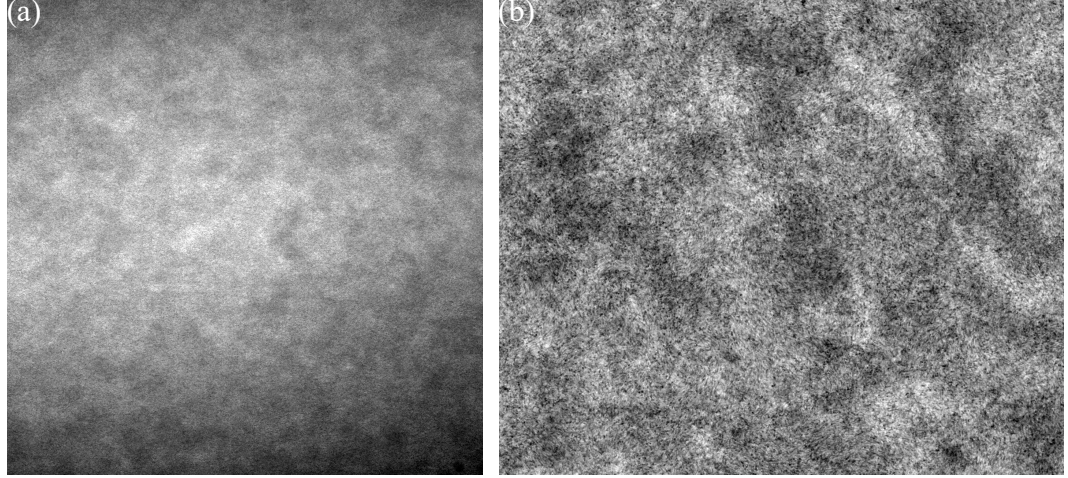


Figure 1.4: Image with (a) and without (b) the diffusion filter (D).

the diffusion filter (D). Without diffusing the illumination light, the resulting image is clearly inhomogeneous in a large range, with a bright center and a dark bottom area. By putting the diffusion filter in the illumination light path, one can make the illumination light much more uniform, as shown in Fig. 1.4b. All the other filters (ND, NCB, PFS) are effectively reducing the overall intensity. Putting in or out these filters only results in globally dimmer or brighter images, without changing the detailed patterns in the image. Thus, these three filters are optional in my experiment. Since powering the light-powered *E. coli* requires a very high light intensity, only the diffusion filter should be kept in the illumination light path.

1.2.2 Avoid over exposure

While high enough light intensity is achieved to power the light-controlled bacteria, the light is so strong that the camera is over exposed and does not record any meaningful signal. In order to power the bacteria, the illumination light intensity cannot be reduced. The only way to avoid the over exposure is to add neutral density filters between the

specimen and the camera, so that the light goes to the camera gets dimmer. Fig. 1.3c and d show how I placed the filters between the specimen and the camera. I took out one of the filter cube from the turret under the objective, which is originally used for fluorescence microscopy. Then I put a piece of neutral density filter on top of the cube and put the cube back to the turret. This additional filter allows for the imaging under strong illumination light.

1.3 Image Analysis

With the fast developments of digital imaging, human are enabled to investigate many processes, ranging from astronomical object motions to microorganism behavior, in unprecedented detail [29]. While it is getting easier than ever to acquire large amount of images, a demand for automated image analysis has also become unprecedented [30, 31, 32].

Particle tracking has been one of the most useful automated image analysis tools in the study of colloids and microorganisms. Over the last 20 years, it has developed significantly and many algorithms, toolkits and all-in-one softwares have been implemented and applied in a variety of image analysis tasks. Despite the abundance of particle tracking tools, no agreement has been made on which one in the vast collection of tools works best. Much effort has been devoted to answer this question by comparing the performance of different tools [29, 33, 34, 35, 36, 37, 38, 39]. In these studies, though different algorithms show different performance, no single algorithm outperforms all the others in all scenarios.

Particle tracking is generally composed of two steps: particle detection (spatial) and linking trajectories (temporal). For the detection step, based on the feature (generalized “particle”) shape sought, different methods are used. For point features, a local maxima finding method is often used; for edge features, group labeling is often used; and for

region features, region seeding is often used [33].

1.3.1 Anisotropic Particle Tracking

A challenge I encountered when working on the diffusion project was the detecting of the ellipsoidal particles surrounded by moving microorganisms (bacteria and algae). A local maxima finding method was applied previously to detect the center of an ellipsoidal particle [40]. Combined with intensity fitting around the center in different directions, the orientation of the particle can also be obtained. The same method, however, does not work well for my image because of the presence of microorganisms, which give rise to many more local maxima in the image (a typical image is shown in Fig. 1.5a). To overcome this challenge, I adapted a thresholding and connected group labeling based method from Ref. [41, 42, 43]. The method has the following steps:

- threshold the grayscale image (Fig. 1.5a) to a binary image (Fig. 1.5b)
- find connected white regions (`skimage.measure.label` in Python)
- find the best-fit ellipse of each white connected regions found in the last step, as indicated by the red ellipses in Fig. 1.5c (`skimage.measure.regionprops` in Python)
- filter the parameters of the ellipses with appropriate criteria, so that only the desired ellipse is found, as indicated by the red ellipse in Fig. 1.5d

Fig. 1.5 only illustrates the essential idea of the method. When applying the method, some necessary image preprocessing, including linear, nonlinear and frequency filters need to be used to make sure the desired features stand out, and the undesired noises are suppressed. The preprocessing techniques have been reviewed in Ref. [33, 32]. This method was used to obtain the trajectories of ellipsoidal particles in algal suspensions,

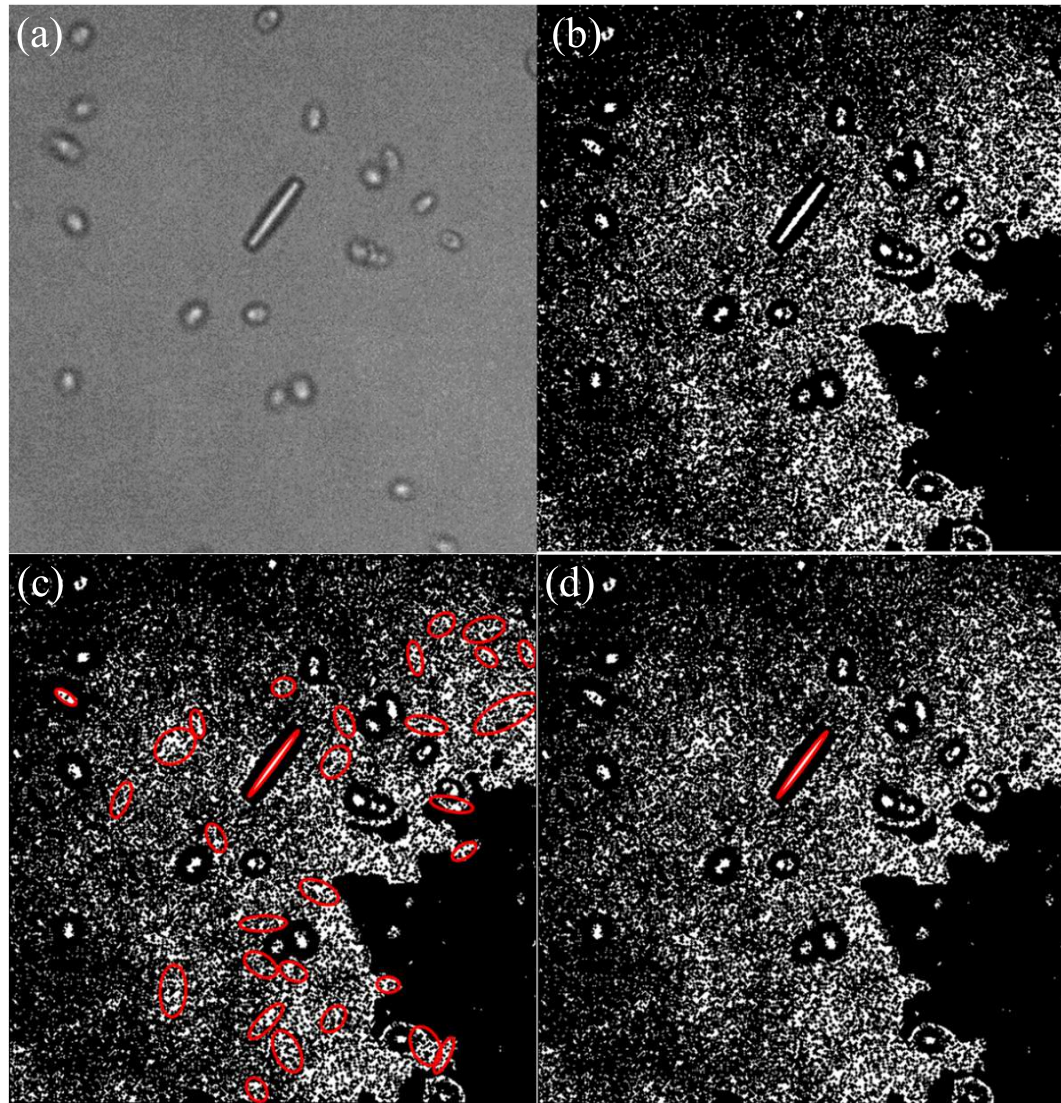


Figure 1.5: Illustration of ellipsoidal particle detection by thresholding and group labeling. (a) The raw image: an ellipsoidal polystyrene particle surrounded by swimming algae in a suspension. (b) Binarized raw image. (c) Detection result of connected white regions. (d) Final result after appropriate filtering.

which was then used to calculate the diffusivity for my first collaborative project, reported in Ref. [44].

1.3.2 Manual Particle Tracking Software: *manTrack*

Despite the great advances of particle tracking techniques, the accuracy suffers much from poor image quality and mutual touching of objects in images, especially when imaging dense suspensions of microorganisms [34]. A very challenging particle detecting task is manifested by a dense suspension of collectively moving bacteria, as shown in Fig. 1.6a. Despite the use of confocal microscopy, most bacteria are seen to be overlapping with others and are in very different shapes, making it impossible for existing tools to detect all the desired features. In a scenario like this, human eyes are the most powerful complementary tool to machines.

Manually marking the positions of particles is feasible when one image only contains one or several particles. When particle numbers get large, however, it is no longer feasible (a typical video I take contains hundreds of particles). I combined the automated tracking and the manual tracking together in order to take the advantages of both: fast and reliable, by implementing a manual tracking software *manTrack* with graphical user interface (GUI). The workflow for using *manTrack* is:

- Use an automated method to do a preliminary particle tracking (or detection).
- Load the preliminary automated detection result into *manTrack*. The result will be displayed in *manTrack* GUI as elliptical contours, as shown in Fig. 1.6b.
- When “delete mode” is enabled, one can delete one entry from the result by clicking on the elliptical contour. In Fig. 1.6c, the entry at the tip of the red arrow has been deleted.

- When “track mode” is enabled, one can add an entry to the current result by drawing an ellipse in the image, as shown by the black contour in Fig. 1.6d.

manTrack provides a user friendly GUI for efficient modification of preliminary automated particle detection results. The combination of machine automated detection and human eye detection makes possible good accuracy and an acceptable execution speed. This software was used for analyzing the orientation of bacteria in active turbulence (Chap. ??).

Several new tools have been developed in recent years, such as *TrackMate* and *tTt* [45, 39]. The fast growth of technologies in other fields, especially artificial intelligence, has stimulate the development of new tracking techniques [46, 47].

1.3.3 Particle Image Velocimetry

Particle image velocimetry (PIV) is a method of visualizing flow using based on images. It is used to obtain instantaneous fluid velocity fields by comparing positions of tracer particles in the fluids in consecutive image frames. The tracer particles are assumed to follow the flow faithfully all the time, and this assumption is in general valid when particle size is small. The degree of how faithful the tracers follow the flow is quantified by Stokes number, which compares the intrinsic relaxation time scale and the characteristic time scale of the flow.

The comparison between two image frames is done by dividing the images in to small interrogation windows and computing the correlations of the two images in these windows, which essentially looks for the similar features between the two images. This procedure is illustrated in Fig. 1.8. Fig. 1.8a and b are two example images and Fig. 1.8c shows the instantaneous flow field obtained from PIV analysis. The result suggests that there is a global flow going to the bottom of the images. Though it is not so obvious in the original images, if we zoom in to a small region, as shown in Fig. 1.8d and e, the

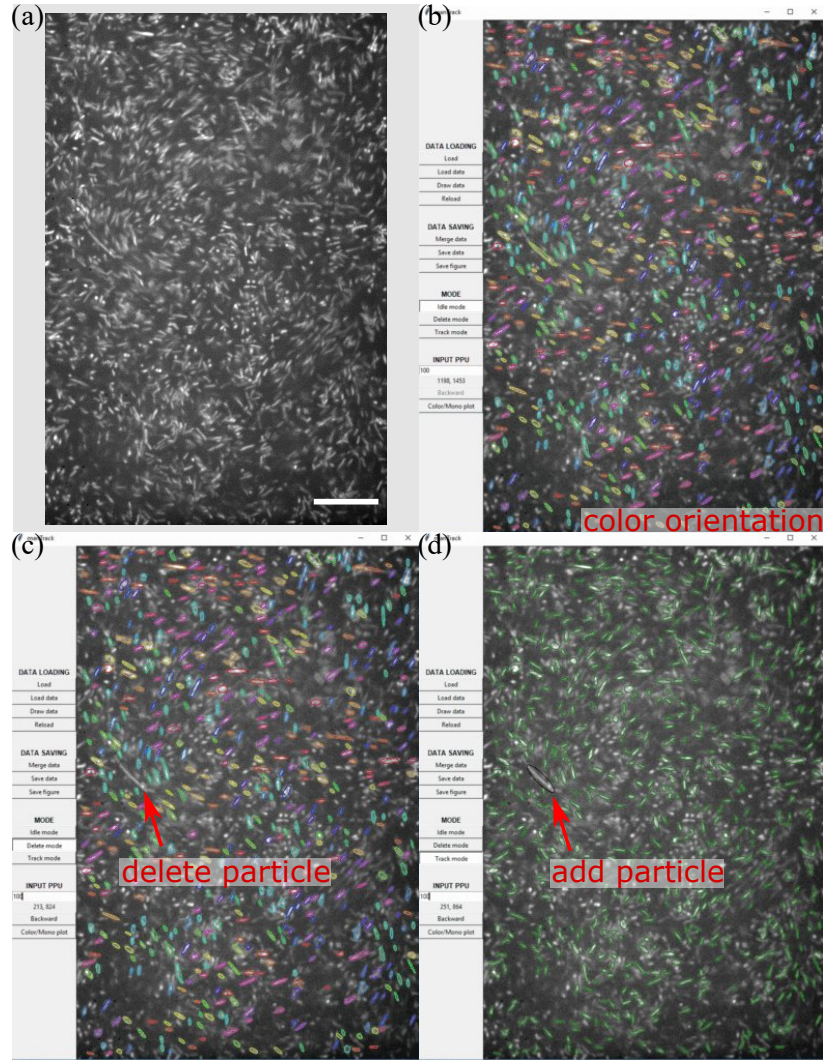


Figure 1.6: A challenging particle detection task and the manual tracking software. (a) Confocal microscopy image of *E. coli* collective motion ($\phi = 6.4\%$). (b)-(d) Snapshots of the manTrack software, demonstrating color-coded orientation, manual deleting and manual adding.

similar features (indicated by red circles) get obvious and we therefore expect the flow going to the bottom of the images, as shown in Fig. 1.8f.

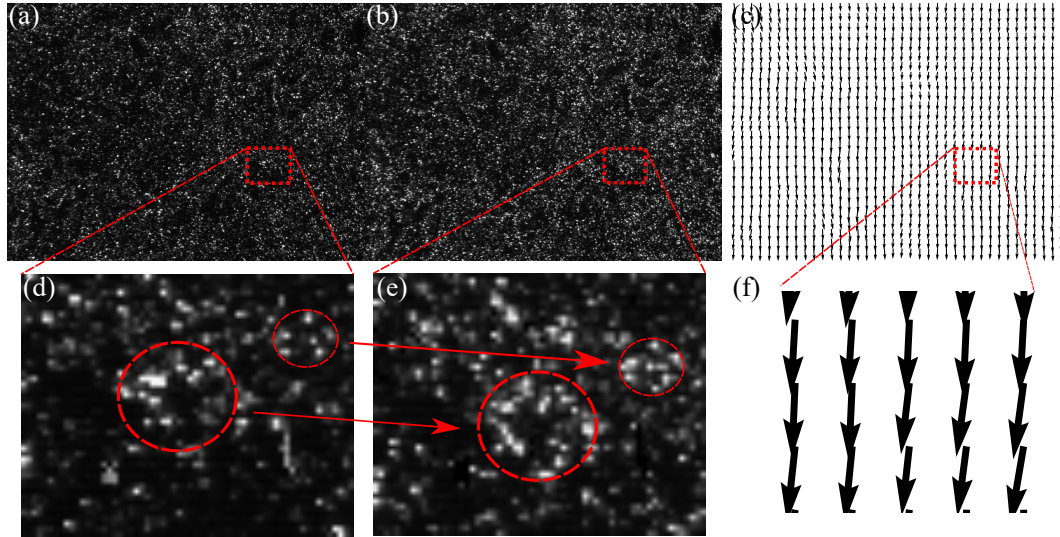


Figure 1.7: **PIV working principle illustration.** (a) and (b) are images of fluid flows seeded with tracer particles. (c) is the instantaneous velocity field in (a) and (b), obtained from PIV. (d) and (e) are zoom-in’s of the two images in a small window. Circles indicates similar image features in (d) and (e). (f) is a zoom-in of velocity field.

Invented in the 1970s, PIV has been developed into a mature flow velocimetry technique today. Several implementations of the algorithm are present in different programming frameworks, such as Matlab, Mathematica and Python. In this work, we use an open source PIV toolkit *OpenPIV* written in Python, which is maintained by Liberzon and co-workers [24, 25].

1.3.4 Spatial and Temporal Correlation Functions

Spatial (temporal) correlation functions describe how variables, such as velocity and density, at different positions (time) are related. It measures the order in a system. These functions are used in the study of giant number fluctuations to measure the characteristic length and time in bacterial suspensions of different volume fractions (Chap. ??).

The correlation functions have been defined clearly in statistical mechanics and mathematics. For example, the spatial correlation function of number density $n(\mathbf{r})$, $C_n(\mathbf{R})$ is

$$C_n(\mathbf{R}) = \frac{\langle n(\mathbf{r}) \cdot n(\mathbf{r} + \mathbf{R}) \rangle - \langle n(\mathbf{r}) \rangle \langle n(\mathbf{r} + \mathbf{R}) \rangle}{\sigma_{n(\mathbf{r})}^2} \quad (1.1)$$

where $\langle A \rangle$ denotes the spatial average of A , and σ_A denotes the standard deviation of A .

Although the definition is clear, the programming implementation can be quite different in efficiency. When implementing these correlation functions, I learned an important trick—code vectorization—which can speed up the computation of correlation functions up to 50 times. The enhancement of performance gets more pronounced when the input data is larger. Therefore, I would like to document this knowledge here.

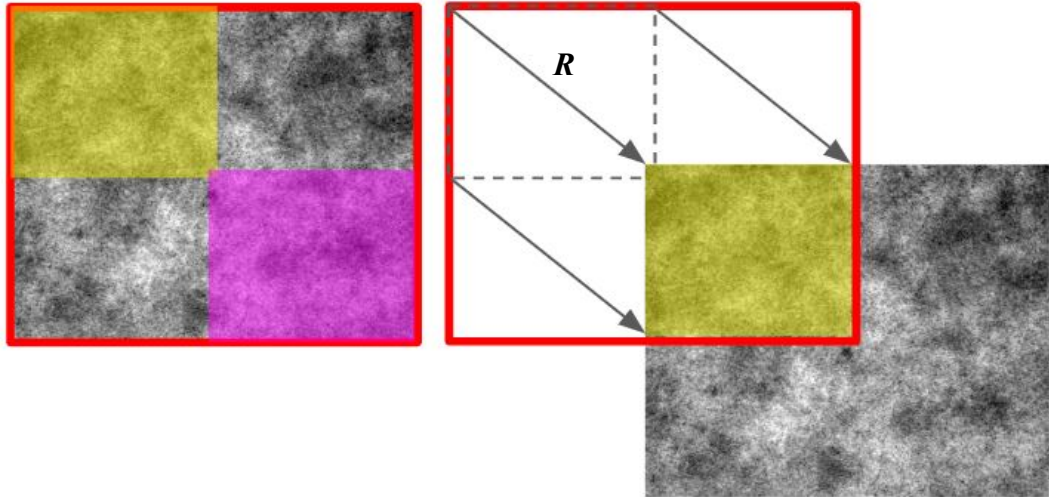


Figure 1.8: Code vectorization illustration. The correlation function at a certain distance \mathbf{R} , $C(\mathbf{R})$ can be calculated without using a `for` loop. Two subspaces are identified from the whole space, as indicated by purple and yellow shaded regions, which are \mathbf{R} away from each other. $C(\mathbf{R})$ can be calculated by taking the product of these two subspaces and then taking the mean of this product.

The calculation of the correlation function in Eq. 1.1 requires going over the whole

space twice: for each point \mathbf{r} in the space, all possible distance \mathbf{R} needs to be examined. In two dimensional space, this procedure leads to four `for` loops. The basic idea of code vectorization is to avoid the extensive use of `for` loops. In this specific case, for every possible distance \mathbf{R} , the correlation can be calculated without using a `for` loop, by directly calculating the product of two subspaces and the taking average, as illustrated in Fig. ???. Two subspaces are identified from the whole space, which are \mathbf{R} away from each other, as indicated by purple and yellow shaded regions. Note that matrix product calculation is well optimized in almost all programming languages and is much faster than looping over every element in a matrix. Using this trick, only two `for` loops are necessary, which go over all possible distances \mathbf{R} . The Python implementations of spatial and temporal correlation functions, as well as a speed comparison between non-vectorized and vectorized programs, can be found in the [Appendix](#).

1.3.5 Energy Spectrum Calculation

As is discussed in Sec. ???, energy spectra have been widely used for studying the flow structure of classic turbulent flows, by revealing the kinetic energy distribution over different length scales. Here, we show the details in the method of calculating energy spectra of the flow in bacterial suspensions at various volume fractions, using the velocity fields obtained from PIV analysis. This calculation will be used in Chap. ?? and Chap. ??.

The energy spectra of bacterial suspensions are calculated as the following

$$E(k_x, k_y) = \frac{\langle u_k(k_x, k_y)u_k^*(k_x, k_y) + v_k(k_x, k_y)v_k^*(k_x, k_y) \rangle}{2A} \quad (1.2)$$

where E is the energy density in k space, u_k and v_k are k space velocity fields, A is the real space area of the system and $*$ denotes the complex conjugate. The $\langle \cdot \rangle$ denotes an

average over multiple images from different times.

The fourier transform of real space velocity u_k and v_k are computed as the following:

- apply the built-in Fast Fourier Transform (FFT) function of Python `numpy.fft` package to the discrete velocity field $v(x, y)$ (from PIV) to get $V_k(k_x, k_y)$
- since the FFT is defined as

$$V_k = \sum_{m=0}^{n-1} v_m \exp(-2\pi i \frac{mk}{n})$$

missing the dx counterpart in the continuous Fourier transform, we additionally multiply d_{step}^2 to $V_k(k_x, k_y)$ to get the wavenumber domain velocity $v_k(k_x, k_y)$

- the wavenumber field k corresponding to $v_k(k_x, k_y)$ is obtained by applying the `numpy.fft.fftfreq` function. Since the definition of FFT introduces a prefactor 2π to the wavenumber, an additional 2π is also multiplied to k

The calculation described above is implemented in a Python code, which can be found in [Appendix](#).

1.3.6 Other Image Analysis Tools

- Particle tracking based on image cross-correlation
- Orientation tracking based on Fast Fourier Transform (FFT)
- Density fluctuation calculations

1.4 Micro-fabrication and Microfluidic Viscometer

1.4.1 Micro-fabrication

We used a standard micro-fabrication technique, soft lithography, to produce the microfluidic viscometer we used in the rheology project (Chap. ??) [48]. Such a fabrication usually involves the following steps: experimental design, pattern design, mask fabrication, master fabrication and elastomeric stamp fabrication. After deciding on using the Y-shaped channel viscometer (Fig. 1.9a) [49], I did the pattern design and the staff at Minnesota Nano Center (MNC) had the mask fabricated for me. With the mask, I fabricated the masters of the Y-shaped channel viscometer for various channel heights using the MNC facilities. Then the masters were used for fabricating elastomeric stamps, using Sylgard 184 Silicone Elastomer Kit (Dow Inc.).

To produce masters for the various channel heights, different photoresists need to be used. I chose the SU-8 3000 series photoresists due to their good adhesion property and reduced coating stress, as well as their ready availability in the MNC labs. SU-8 3025 was used for channel heights from 25 to 50 μm . SU-8 3050 was used for channel heights from 50 to 128 μm . Following the procedures described in the photoresist manual, which includes substrate preparation, spin coating, soft bake, exposure, post exposure bake and develop, a photoresist patterned silicon wafer can be produced (Fig. 1.9b).

The elastomeric stamp is fabricated by pouring the Sylgard 184 Silicone Elastomer Kit, which contains a base and a crosslinker in a volume ratio 10:1, onto the photoresist masters. After curing for 3 hours at 70 °C, the pattern of the master mold was perfectly replicated on the solidified elastomer. Finally, a piece of coverslip was stuck on the patterned side of the elastomer by plasma cleaning the surfaces of both. The microfluidic channel is shown in Fig. 1.9c. The length and width of the two arms are 1 cm and 300 μm , respectively. The length and width of the main channel are 4 cm and 600 μm ,

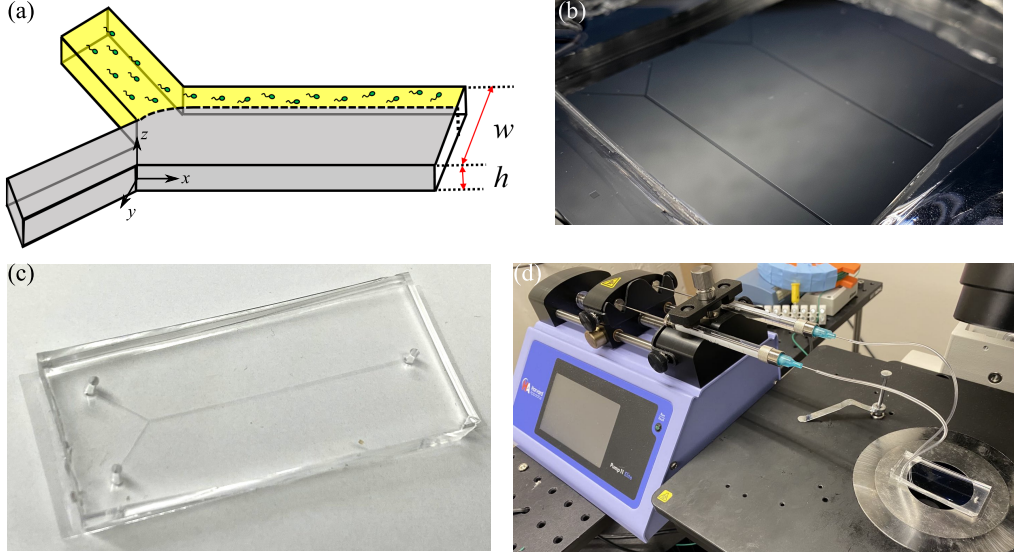


Figure 1.9: Microfluidic viscometer fabrication and setup. (a) A sketch of the Y-shaped channel microfluidic viscometer. (b) Master mold of the channel. (c) PDMS Y-shaped channel microfluidic viscometer. (d) Viscometer connected to a syringe pump by plastic tubes, placed on Nikon inverted microscope specimen stage.

respectively. The height of the channel h ranges from $25 \mu\text{m}$ to $128 \mu\text{m}$. Two cylindrical holes were punched at the ends of the two arms so that fluids can be pumped in.

1.4.2 Microfluidic Viscometer

To use the elastomeric stamp as a microfluidic viscometer, we connected it with a precision syringe pump (Harvard Apparatus, Elite 11) through elastic tubes, as shown in Fig. 1.9. The two syringes contained two different fluids: one was the bacterial suspension with viscosity to be measured, and the other was a reference fluid with known viscosity, typically water. The two fluids were pumped into the viscometer at the same volumetric flow rate Q .

The working principle of the viscometer is that thicker fluids flow slower than thinner ones. More formally, if we examine a fluid with viscosity η , driven by a pressure gradient

dp/dx to flow in the x -direction between two parallel no-slip boundaries at $z = \pm h/2$, as shown in Fig. 1.9a. At low Reynolds number limit, the flow rate regime of interest, the flow is governed by Navier-Stokes equation

$$0 = -\frac{dP}{dx} + \eta \frac{d^2 u_x}{dz^2} \quad (1.3)$$

The resulting flow is parabolic in x - z plane and is approximately constant in y -direction, and can be described by Eq. 1.4

$$u_x(z) = \frac{1}{2\eta} \frac{dP}{dx} \left(\frac{y^2}{h^2} - \frac{1}{4} \right) \quad (1.4)$$

For two different fluids with viscosities η_1 and η_2 , the mean flow velocity in x -direction $\langle u_1 \rangle$ and $\langle u_2 \rangle$ are related to each other by

$$\frac{\langle u_1 \rangle}{\langle u_2 \rangle} = \frac{\eta_2}{\eta_1} \quad (1.5)$$

noting that the flow rate $Q = \langle u \rangle dh$, where d is the width (y -direction) of the flow, we can substitute the velocities $\langle u_1 \rangle$ and $\langle u_2 \rangle$ in Eq. 1.5 to get

$$\frac{d_1}{d_2} = \frac{\eta_1}{\eta_2} \quad (1.6)$$

Eq. 1.6 is the working equation of the microfluidic viscometer. By imaging and measuring the width d_1 and d_2 of the two fluids in the channel, and combining the known viscosity of the reference fluid η_2 , we can measure η_1 .

1.5 Light-controlled *E. coli*: Genetic Modification and Culturing

Controlling the swimming speed of swimmers can enormously expand the capability of experimental active fluid investigations. Our lab used to exploit a “negative phototaxis” property of a mutant *E. coli* strain to control its swimming speed. The mutant strain carries a *hemH* gene knockout, so that it accumulates protoporphyrin IX. When exposed to blue light, protoporphyrin IX catalyzes the production of H₂O₂, which causes the “negative chemotaxis” tumbling response of the *E. coli* mutant [50]. Although this mutant strain enables us to reduce the swimming speed, the recovery of swimming speed remains challenging due to the excessive production and accumulation of toxic H₂O₂. Hence, some important experiments, such as the study of the onset of active turbulence, which will be detailed in Chap. ??, cannot be done with this strain.

An alternative mechanism that can be exploited to control bacterial swimming speed is to introduce a light-driven proton pump protein, proteorhodopsin (PR), to *E. coli*. PR protein has been found in marine micro-organisms [1, 3], and has recently been successfully expressed in *E. coli* [4]. In contrast to the *hemH* knockout mutant, PR is much less harmful and provides better recovery of swimming speed. Therefore, I transformed the wildtype *E. coli* K-12 strain BW25113 (Ref. [51]) with a plasmid pZE-PR containing the gene that encoded the PR protein. The sequence of the PR gene was found in Ref. [3] and was synthesized by Eurofins Scientific. The plasmid was constructed by the standard protocol consisting of PCR, enzymatic digestion and ligation. The PCR was carried out with Phusion High-Fidelity DNA polymerase (New England BioLabs) according to the manufacturer’s instructions. Both the plasmid vector pZE and the PR gene were digested with Acc651-Xba1, and were subsequently ligated. XL10-Gold *E. coli* strain was used for cloning the plasmid. Finally, the wildtype strain BW25113

was transformed with the plasmid by electro-poration and the light-controlled *E. coli* mutant strain was constructed. The details of bacterial strains, plasmids and primers used in this work are listed in Table. 1.2.

| Name | Relevant genotype or sequence | | | Reference |
|-----------------|--|--------------------------------|-------------------------------|------------|
| <i>Strains</i> | | | | |
| BW25113 | $rrnB_{T14}$ | $\Delta lacZ_{WJ16} hsdR514$ | $\Delta araBAD_{AH33}$ | [51] |
| | $\Delta rhaBAD_{LD78}$ | | | |
| XL10-Gold | Tet ^R | $\Delta(mcrA)183$ | $\Delta(mcrCB-hsaSMR-mrr)173$ | Stratagene |
| | | <i>endAlsupE44 thi-l recAl</i> | | |
| <i>Plasmids</i> | | | | |
| pZE-PR | ColE1 origin, Amp ^R , P _L lacO ₁ : PR | | | This work |
| <i>Primers</i> | | | | |
| PR-Acc651-F | CCCGGGGGTACCATGAAGTTGTTGATCTTGGGAT | | | |
| PR-Xba1-R | CCCGGGTCTAGATTATGCGTCGATGACTCTTCACG | | | |

Table 1.2: Strains, plasmids and primers.

The chromophore retinal molecule is essential for the PR protein to function as a proton pump. The retinal is isomerized upon illumination, and in this way it drives the proton transportation across cell membrane [2]. *E. coli* does not synthesize such molecules. In order to activate the function of PR in *E. coli*, we need to supplement the culturing media of *E. coli* with retinal, in the form of ethanol solution of all-trans-retinal (Sigma-Aldrich). Typically, a 10 mM all-trans-retinal solution is prepared as a stock solution. When supplementing the culturing media, 1/1000 volume of retinal solution is used to achieve a final concentration 10 μ M. To trigger the expression of PR gene under a P_Llac operon, we also need to supplement the culturing media with another chemical Isopropyl β -D-1-thiogalactopyranoside (IPTG, Sigma-Aldrich) at a final concentration 1 mM. Therefore, when culturing the light-controlled *E. coli*, an additional step needs to be added to the standard protocol (described in Sec. 1.1.2) between step 2(c) and 2(d). Typically, 3 hours after step 2(c), retinal and IPTG are supplemented to the culturing media.

Bibliography

- [1] O. Beja, L. Aravind, E. V. Koonin, M. T. Suzuki, A. Hadd, L. P. Nguyen, S. B. Jovanovich, C. M. Gates, R. A. Feldman, J. L. Spudich, E. N. Spudich, and E. F. DeLong. Bacterial rhodopsin: Evidence for a new type of phototrophy in the sea. *Science*, 289(5486):1902–1906, 2000.
- [2] Sriram Subramaniam and Richard Henderson. Molecular mechanism of vectorial proton translocation by bacteriorhodopsin. *Nature*, 406(6796):653–657, 2000, NIHMS150003.
- [3] José R. De la Torre, Lynne M. Christianson, Oded Béjà, Marcelino T. Suzuki, David M. Karl, John Heidelberg, and Edward F. DeLong. Proteorhodopsin genes are distributed among divergent marine bacterial taxa. *Proceedings of the National Academy of Sciences of the United States of America*, 100(22):12830–12835, 2003.
- [4] Jessica M. Walter, Derek Greenfield, Carlos Bustamante, and Jan Liphardt. Light-powering *Escherichia coli* with proteorhodopsin. *Proceedings of the National Academy of Sciences of the United States of America*, 104(7):2408–2412, 2007.
- [5] Nico J. Claassens, Michael Volpers, Vitor A.P.Martins dos Santos, John Van der Oost, and Willem M. de Vos. Potential of proton-pumping rhodopsins: Engineering photosystems into microorganisms. *Trends in Biotechnology*, 31(11):633–642, 2013.

- [6] W. C.K. Poon. From Clarkia to escherichia and janus: The physics of natural and synthetic active colloids. *Proceedings of the International School of Physics "Enrico Fermi"*, 184:317–386, 2012, 1306.4799.
- [7] Jana Schwarz-Linek, Jochen Arlt, Alys Jepson, Angela Dawson, Teun Vissers, Dario Miroli, Teuta Pilizota, Vincent A. Martinez, and Wilson C.K. Poon. Escherichia coli as a model active colloid: A practical introduction. *Colloids and Surfaces B: Biointerfaces*, 137:2–16, 2016, 1506.04562.
- [8] Eric Lauga. Bacterial Hydrodynamics. *Annual Review of Fluid Mechanics*, 48:105–130, 2016, 1509.02184.
- [9] J. Elgeti, R. G. Winkler, and G. Gompper. Physics of microswimmers - Single particle motion and collective behavior: A review. *Reports on Progress in Physics*, 78(5), 2015, 1412.2692.
- [10] Aditi R. Simha and Sriram Ramaswamy. Hydrodynamic fluctuations and instabilities in ordered suspensions of self-propelled particles. *Physical review letters*, 89(5):058101, 2002, 0108301.
- [11] Takuji Ishikawa and T. J. Pedley. The rheology of a semi-dilute suspension of swimming model micro-organisms. *Journal of Fluid Mechanics*, 588:399–435, 2007.
- [12] David Saintillan and Michael J. Shelley. Instabilities and pattern formation in active particle suspensions: Kinetic theory and continuum simulations. *Physical Review Letters*, 100(17):1–4, 2008.
- [13] David Saintillan and Michael J. Shelley. Instabilities, pattern formation, and mixing in active suspensions. *Physics of Fluids*, 20(12), 2008.

- [14] Knut Drescher, Jörn Dunkel, Luis H. Cisneros, Sujoy Ganguly, and Raymond E. Goldstein. Fluid dynamics and noise in bacterial cell-cell and cell-surface scattering. *Proceedings of the National Academy of Sciences of the United States of America*, 108(27):10940–10945, 2011.
- [15] Linda Turner, William S. Ryu, and Howard C. Berg. Real-time imaging of fluorescent flagellar filaments. *Journal of Bacteriology*, 182(10):2793–2801, 2000.
- [16] D. T.N. Chen, A. W.C. Lau, L. A. Hough, M. F. Islam, M. Goulian, T. C. Lubensky, and A. G. Yodh. Fluctuations and rheology in active bacterial suspensions. *Physical Review Letters*, 99(14):1–4, 2007, 0709.1465.
- [17] Alison E. Patteson, Arvind Gopinath, Prashant K. Purohit, and Paulo E. Arratia. Particle diffusion in active fluids is non-monotonic in size. *Soft Matter*, 12(8):2365–2372, 2016, 1505.05803.
- [18] T. V. Kasyap, Donald L. Koch, and Mingming Wu. Hydrodynamic tracer diffusion in suspensions of swimming bacteria. *Physics of Fluids*, 26(8), 2014.
- [19] Alys Jepson, Vincent A. Martinez, Jana Schwarz-Linek, Alexander Morozov, and Wilson C.K. Poon. Enhanced diffusion of nonswimmers in a three-dimensional bath of motile bacteria. *Physical Review E - Statistical, Nonlinear, and Soft Matter Physics*, 88(4):3–7, 2013, 1307.1274.
- [20] Gastón Miño, Thomas E. Mallouk, Thierry Darnige, Mauricio Hoyos, Jeremi Dauchet, Jocelyn Dunstan, Rodrigo Soto, Yang Wang, Annie Rousselet, and Eric Clement. Enhanced diffusion due to active swimmers at a solid surface. *Physical Review Letters*, 106(4):1–4, 2011, 1012.4624.
- [21] Alan J. Hargreaves Philip L.R. Bonner. *Basic Bioscience Laboratory Techniques: A Pocket Guide*. 2011.

- [22] Yi Peng, Lipeng Lai, Yi Shu Tai, Kechun Zhang, Xinliang Xu, and Xiang Cheng. Diffusion of ellipsoids in bacterial suspensions. *Physical Review Letters*, 116(6):1–5, 2016, 1509.05893.
- [23] Nikon Instruments Inc. Nikon inverted microscope eclipse ti-e ti-e/b instructions: <http://squishycell.uchicago.edu/manuals/ti-e>
- [24] Z. J. Taylor, R. Gurka, G. A. Kopp, and A. Liberzon. Openpiv official website: <http://www.openpiv.net/>.
- [25] Z. J. Taylor, R. Gurka, G. A. Kopp, and A. Liberzon. Long-duration time-resolved piv to study unsteady aerodynamics. *IEEE Transactions on Instrumentation and Measurement*, 59(12):3262–3269, 2010.
- [26] Casper van der Wel, Daniel Allan, Nathan Keim, and Thomas Caswell. trackpy official website: <http://soft-matter.github.io/trackpy/v0.4.2/>.
- [27] John C. Crocker and Eric R. Weeks. Particle tracking using idl: <http://www.physics.emory.edu/faculty/weeks//idl/index.html>.
- [28] Daniel Blair and Eric Dufresne. The matlab particle tracking code repository: <http://site.physics.georgetown.edu/matlab/>.
- [29] Yannis Kalaidzidis. Intracellular objects tracking. *European Journal of Cell Biology*, 86(9):569–578, 2007.
- [30] Erik Meijering, Ihor Smal, and Gaudenz Danuser. Tracking in molecular bioimaging. *IEEE Signal Processing Magazine*, 23(3):46–53, 2006.
- [31] Khuloud Jaqaman, Dinah Loerke, Marcel Mettlen, Hirotaka Kuwata, Sergio Grinstein, Sandra L. Schmid, and Gaudenz Danuser. Robust single-particle tracking in live-cell time-lapse sequences. *Nature Methods*, 5(8):695–702, 2008.

- [32] Karl Rohr, William J. Godinez, Nathalie Harder, Stefan Wörz, Julian Mattes, Wolfgang Tvarusko, and Roland Eils. Tracking and quantitative analysis of dynamic movements of cells and particles. *Cold Spring Harbor Protocols*, 5(6):1–17, 2010.
- [33] Jonas F. Dorn, Gaudenz Danuser, and Ge Yang. Computational Processing and Analysis of Dynamic Fluorescence Image Data. *Methods in Cell Biology*, 85(08):497–538, 2008.
- [34] Erik Meijering, Oleh Dzyubachyk, Ihor Smal, and Wiggert A. van Cappellen. Tracking in cell and developmental biology. *Seminars in Cell and Developmental Biology*, 20(8):894–902, 2009.
- [35] Ihor Smal, Marco Loog, Wiro Niessen, and Erik Meijering. Quantitative comparison of spot detection methods in fluorescence microscopy. *IEEE Transactions on Medical Imaging*, 29(2):282–301, 2010.
- [36] Erik Meijering, Oleh Dzyubachyk, and Ihor Smal. *Methods for cell and particle tracking*, volume 504. Elsevier Inc., 1 edition, 2012.
- [37] Nicolas Chenuard, Ihor Smal, Fabrice De Chaumont, Martin Maška, Ivo F. Sbalzarini, Yuanhao Gong, Janick Cardinale, Craig Carthel, Stefano Coraluppi, Mark Winter, Andrew R. Cohen, William J. Godinez, Karl Rohr, Yannis Kalaidzidis, Liang Liang, James Duncan, Hongying Shen, Yingke Xu, Klas E.G. Magnusson, Joakim Jaldén, Helen M. Blau, Perrine Paul-Gilloteaux, Philippe Roudot, Charles Kervrann, François Waharte, Jean Yves Tinevez, Spencer L. Shorte, Joost Willemse, Katherine Celler, Gilles P. Van Wezel, Han Wei Dan, Yuh Show Tsai, Carlos Ortiz De Solórzano, Jean Christophe Olivo-Marin, and

- Erik Meijering. Objective comparison of particle tracking methods. *Nature Methods*, 11(3):281–289, 2014.
- [38] Martin Maška, Vladimír Ulman, David Svoboda, Pavel Matula, Petr Matula, Cristina Ederra, Ainhoa Urbiola, Tomás España, Subramanian Venkatesan, Deepak M.W. Balak, Pavel Karas, Tereza Bolcková, Markéta Štreitová, Craig Carthel, Stefano Coraluppi, Nathalie Harder, Karl Rohr, Klas E.G. Magnusson, Joakim Jaldén, Helen M. Blau, Oleh Dzyubachyk, Pavel Křížek, Guy M. Hagen, David Pastor-Escuredo, Daniel Jimenez-Carretero, Maria J. Ledesma-Carbayo, Arrate Muñoz-Barrutia, Erik Meijering, Michal Kozubek, and Carlos Ortiz-De-Solorzano. A benchmark for comparison of cell tracking algorithms. *Bioinformatics*, 30(11):1609–1617, 2014.
- [39] Oliver Hilsenbeck, Michael Schwarzfischer, Stavroula Skylaki, Bernhard Schauberger, Philipp S. Hoppe, Dirk Loeffler, Konstantinos D. Kokkaliaris, Simon Hastreiter, Eleni Skylaki, Adam Filipczyk, Michael Strasser, Felix Buggenthin, Justin S. Feigelman, Jan Krumsiek, Adrianus J.J. Van Den Berg, Max Endele, Martin Etzrodt, Carsten Marr, Fabian J. Theis, and Timm Schroeder. Software tools for single-cell tracking and quantification of cellular and molecular properties. *Nature Biotechnology*, 34(7):703–706, 2016.
- [40] Y. Han, A. M. Alsayed, M. Nobili, J. Zhang, T. C. Lubensky, and A. G. Yodh. Brownian motion of an ellipsoid. *Optics InfoBase Conference Papers*, (October):626–631, 2006.
- [41] F. Boulogne. Custom feature detection and velocity fields: Bubble tracking in 2d foams: <http://soft-matter.github.io/trackpy/v0.4.2/tutorial/custom-feature-detection.html>.

- [42] A. Sauret, F. Boulogne, J. Cappello, E. Dressaire, and H. A. Stone. Damping of liquid sloshing by foams. *Physics of Fluids*, 27(2), 2015, 1411.6542.
- [43] J. Cappello, A. Sauret, F. Boulogne, E. Dressaire, and H. A. Stone. Damping of liquid sloshing by foams: from everyday observations to liquid transport. *Journal of Visualization*, 18(2):269–271, 2015, 1411.2123.
- [44] O. Yang, Y. Peng, Z. Liu, C. Tang, X. Xu, and X. Cheng. Dynamics of ellipsoidal tracers in swimming algal suspensions. *Physical Review E*, 94(4), 2016.
- [45] Jean Yves Tinevez, Nick Perry, Johannes Schindelin, Genevieve M. Hoopes, Gregory D. Reynolds, Emmanuel Laplantine, Sebastian Y. Bednarek, Spencer L. Shorte, and Kevin W. Eliceiri. TrackMate: An open and extensible platform for single-particle tracking. *Methods*, 115:80–90, 2017.
- [46] Jay M. Newby, Alison M. Schaefer, Phoebe T. Lee, M. Gregory Forest, and Samuel K. Lai. Convolutional neural networks automate detection for tracking of submicron-scale particles in 2D and 3D. *Proceedings of the National Academy of Sciences of the United States of America*, 115(36):9026–9031, 2018, 1704.03009.
- [47] Erick Moen, Dylan Bannon, Takamasa Kudo, William Graf, Markus Covert, and David Van Valen. Deep learning for cellular image analysis. *Nature Methods*, 16(12):1233–1246, 2019.
- [48] Dong Qin, Younan Xia, and George M. Whitesides. Soft lithography for micro- and nanoscale patterning. *Nature Protocols*, 5(3):491–502, 2010.
- [49] Jérémie Gachelin, Gastón Miño, Hélène Berthet, Anke Lindner, Annie Rousselet, and Éric Clément. Non-newtonian viscosity of escherichia coli suspensions. *Physical Review Letters*, 110(26):1–5, 2013, 1210.2102.

- [50] Hanjing Yang, Hachiro Inokuchi, and Julius Adler. Phototaxis away from blue light by an Escherichia coli mutant accumulating protoporphyrin IX. *Proceedings of the National Academy of Sciences of the United States of America*, 92(16):7332–7336, 1995.
- [51] Kirill A. Datsenko and Barry L. Wanner. One-step inactivation of chromosomal genes in Escherichia coli K-12 using PCR products. *Proceedings of the National Academy of Sciences of the United States of America*, 97(12):6640–6645, 2000.